Monthly Notices
of the
ROYAL ASTRONOMICAL SOCIETY

MNRAS **500,** L37–L41 (2021)
Advance Access publication 2020 October 31

doi:10.1093/mnrasl/slaa178

The distribution of neutral hydrogen in the colour–magnitude plane of galaxies

Saili Dutta ★ and Nishikanta Khandai ★

School of Physical Sciences, National Institute of Science Education and Research, HBNI, Jatni 752050, India

Accepted 2020 October 27. in original form 2020 September 30

ABSTRACT

We present the conditional H I (neutral hydrogen) mass function (HIMF) conditioned on observed optical properties, M_r (r-band absolute magnitude), and C_{ur} ($u - r$ colour), for a sample of 7709 galaxies from Arecibo Legacy Fast ALFA (40 per cent data release – α.40) which overlaps with a common volume in SDSS DR7. Based on the conditional HIMF, we find that the luminous red, luminous blue, and faint blue populations dominate the total HIMF at the high-mass end, knee, and the low-mass end, respectively. We use the conditional HIMF to derive the underlying distribution function of $\Omega_{\rm H\,I}$ (H I density parameter), $p(\Omega_{\rm H\,I})$, in the colour–magnitude plane of galaxies. The distribution, $p(\Omega_{\rm H\,I})$, peaks in the blue cloud at $M_r{}^{\rm max} = -19.25$, $C_{ur}{}^{\rm max} = 1.44$ but is skewed. It has a long tail towards faint blue galaxies, and luminous red galaxies. We argue that $p(\Omega_{\rm H\,I})$ can be used to reveal the underlying relation between cold gas, stellar mass, and the star formation rate in an unbiased way, that is, the derived relation does not suffer from survey or sample selection.

Key words: surveys – galaxies: evolution – galaxies: formation – galaxies: luminosity function, mass function – radio lines: galaxies.

1 INTRODUCTION

Cold gas represents an important baryonic component of galaxies since it indicates the amount of gas that is available for future star formation of galaxies. Observationally the star formation surface density is strongly correlated with the cold gas (neutral hydrogen: sum of atomic, H I, and molecular, H_2) surface density in late type disc galaxies – the Kennicutt–Schmidt (KS) law (Schmidt 1959, 1963; Kennicutt 1989, 1998) for star formation. Targeted observations have detected H I in late-type (E and S0) galaxies (Morganti et al. 2006; Oosterloo et al. 2007; Serra et al. 2012), but their star formation rate is negligible to construct a corresponding KS-like law for them. Blind surveys on the other hand have constrained the H I (neutral hydrogen) mass function (HIMF) in the local Universe (Zwaan et al. 2003; Martin et al. 2010; Haynes et al. 2011; Jones et al. 2018), but the HIMF does not reveal how H I is distributed amongst different galaxy populations.

Although the HIMF, and other one-dimensional functions [e.g. multiband luminosity functions, stellar mass functions, star formation rate (SFR) function, to name a few] are important distributions which any theory of galaxy formation should reproduce, they only represent marginalized distributions of higher dimensional multivariate distribution functions of galaxies. These multivariate functions encode the effects and interplay of complex processes between various baryonic components of galaxies. With the advent of ongoing and future large surveys which target different bands of the electromagnetic spectrum there is a need to go beyond one-dimensional functions. It is common to present bivariate or multivariate functions, when the observables are from different surveys, as conditional functions. The bivariate H I mass–B-band luminosity function was estimated from a sample of 61 galaxies in the blind Arecibo H I Strip Survey (Zwaan, Briggs & Sprayberry 2001). More recently, Lemonias et al. (2013) presented the H I mass–stellar mass bivariate function using a parent sample of 480 galaxies from the GALEX Arecibo SDSS Survey (GASS) Data Release 2 (Catinella et al. 2010, 2012).

In this work, we present the conditional HIMF conditioned on optical colour and magnitude using a sample of 7709 galaxies from the blind Arecibo Legacy Fast ALFA (ALFALFA) survey. We then use the conditional HIMF to estimate, for the first time, the two-dimensional distribution function of $\Omega_{\rm H\,I}$ in the colour–magnitude (CM) plane of galaxies. Our paper is organized as follows: we describe our data in Section 2 followed by a brief description of estimating the HIMF in Section 3. We present our results in Section 4 and discuss our results in Section 5. We assume the following cosmology: $\{\Omega_\Lambda, \Omega_{\rm m}, h\} = \{0.7, 0.3, 0.7\}$.

2 DATA

We give a brief summary of our sample, which is based on the α.40 data release of ALFALFA (Haynes et al. 2011) and is the same as in Dutta, Khandai & Dey (2020) (hereafter, D20). We choose an area overlapping with the SDSS DR7 (Abazajian et al. 2009) footprint and the α.40 sample and restrict the redshift range to $cz_{\rm cmb} = 15000\,{\rm km\,s^{-1}}$, to avoid radio frequency interference (RFI). This common volume is $\sim 2.02 \times 10^6$ Mpc^3, and subtends an angular area of ~ 2093 deg^2. We also consider only Code 1 objects, which have a signal-to-noise ratio, SNR > 6.5. Finally, we apply the 50 per cent completeness cut as described in Haynes et al.

★ E-mail: sailidutta@niser.ac.in (SD); nkhandai@niser.ac.in (NK)

(2011), which brings our final sample to 7857 galaxies. Of these, 7709 galaxies (or 98 per cent) have optical counterparts in SDSS and we loosely refer to the remaining 148 (2 per cent) galaxies as *dark* galaxies. In D20, we showed that the dark galaxies contribute about ~ 3 per cent to $\Omega_{\rm H\,I}$. Our results should therefore not be sensitive to this population of dark galaxies. Of the 7709 galaxies that have optical counterparts in SDSS DR7, we use their *ugriz* model magnitudes (extinction corrected) and redshifts to obtain absolute magnitudes (M_u, M_g, M_r, M_i, M_z) using *kcorrect* (Blanton & Roweis 2007). The SDSS galaxy distribution in the CM plane is bimodal. The dot–dashed curve in Fig. 3 is the optimal divider to classify these galaxies into red (above curve) and blue (below curve) populations (Baldry et al. 2004). A bimodal distribution is not seen in our H I-selected sample (Fig. 3) because ALFALFA primarily samples the blue cloud, but is nevertheless seen in SDSS for the volume considered here (see fig. 3 of D20) and we refer to them accordingly as red and blue galaxies. We restrict our study to the $\alpha.40$ rather than the recently released 100 per cent catalogue ($\alpha.100$) (Haynes et al. 2018). This is because we find that at lower declinations, which are now covered by $\alpha.100$, many galaxies have luminous foreground stars (as seen in the images) and photometric values are not available since SDSS has masked these regions. We will consider the $\alpha.100$ sample in the future.

3 ESTIMATION OF HIMF

The HIMF, $\phi(M_{\rm H\,I})$, represents the underlying number density of galaxies in the Universe as a function of their H I mass. This is written as

$$\phi(M_{\rm H\,I}) = \frac{{\rm d}N}{V\,{\rm d}\log_{10} M_{\rm H\,I}}. \quad (1)$$

Here, dN is the number of galaxies with masses in the range $[\log_{10}M_{\rm H\,I}, \log_{10}M_{\rm H\,I} + {\rm dlog}_{10}M_{\rm H\,I}]$ and V is the survey volume of interest. A single Schechter function has been shown to describe the HIMF reasonably well (Zwaan et al. 2003; Martin et al. 2010; Haynes et al. 2011; Jones et al. 2018, D20):

$$\phi(M_{\rm HI}) = \ln(10)\,\phi_*\left(\frac{M_{\rm HI}}{M_*}\right)^{\alpha+1}\exp\left(-\frac{M_{\rm HI}}{M_*}\right), \quad (2)$$

where, ϕ_* is the amplitude, α is the slope at the low-mass end, and M_* is the knee of the HIMF, beyond which the galaxy counts drop exponentially. Converting the observed counts of galaxies to the HIMF is non-trivial. ALFALFA being a blind survey, its sensitivity affects the observed counts. In the context of ALFALFA the sensitivity limit depends both on the galaxy flux and velocity width W_{50}. However, the data of ALFALFA is large enough so that it can be used itself to estimate the completeness limit (Haynes et al. 2011). We use the 50 per cent completeness curve (Haynes et al. 2011) as our sensitivity limit.

We use the two-dimensional stepwise maximum likelihood (2DSWML) method (Loveday 2000; Zwaan et al. 2003; Martin et al. 2010; Haynes et al. 2011) to estimate the HIMF. The 2DSWML estimator is based on the assumption that the observed sample of galaxies is drawn from an underlying distribution function. In our case, it is a bivariate H I mass–velocity width function, $\phi(M_{\rm H\,I}, W_{50})$. The advantage of this method is that it is less susceptible to effects of large-scale structures (e.g. clustering) and the stepwise nature of the method does not assume a functional form but rather estimates ϕ_{jk}. Here $\phi_{jk} \equiv \phi(M^j_{\rm HI}, W^k_{50})$ is the discretised version of bivariate function $\phi(M_{\rm H\,I}, W_{50})$ in bins of mass, $M^j_{\rm HI}$ and velocity width W^k_{50}. As with any maximum likelihood method, the normalization is lost and has to be fixed separately. We use the method outlined in the appendix of D20 to fix the normalization. One can then integrate $\phi(M^j_{\rm HI}, W^k_{50})$ over the velocity width to obtain the HIMF $\phi(M^j_{\rm HI})$ (Zwaan et al. 2003; Martin et al. 2010; Haynes et al. 2011; Jones et al. 2018) or integrate over the mass to obtain $\phi(W^k_{50})$.

We estimate errors in the same manner as in D20. The error in mass is related to the errors in the observed flux (S_{21}) and the errors in distance (D) of each galaxy, since $M_{\rm H\,I}\propto S_{21}D^2$. Based on the observed values and the estimated errors on both flux and distance, we generate 300 Gaussian random realizations for each object in the catalogue. These are then used to quote an error for $\phi(M^j_{\rm HI})$. The second source of errors are Poisson errors which affects the low- and high-mass end of the H I catalogue, both of which have few objects. Finally, we estimate sample variance by splitting the survey area into 26 contiguous regions of approximately equal area. We compute the HIMF for each of these jackknife samples by removing one region at a time. This is then used to compute the jackknife uncertainty. One may consider other sources of errors (see Jones et al. 2018) but as discussed in D20, these may be correlated. For this work, we consider the errors outlined above which are consistent with Martin et al. (2010) and Haynes et al. (2011).

4 RESULTS

We now present the results of our paper. Given that 98 per cent of the H I selected galaxies have optical counterparts a natural question would be to look at the conditional HIMF, conditioned on an optical property. The 2 per cent of galaxies which are dark contribute only 3 per cent to $\Omega^{\rm tot}_{\rm HI}$ (D20). In the rest of the paper, we will therefore ignore this population of dark galaxies since we do not expect them to affect our results quantitatively. We emphasize that this is an H I selected sample for which optical properties exist for all galaxies. Therefore when computing the HIMF (conditioned on an optical property) we need to consider only the ALFALFA selection function and volume. In what follows, we will compute the HIMF based M_r and C_{ur} thresholds.

4.1 Conditional HIMF

We define the colour-conditioned HIMF as

$$\phi(M_{\rm HI}|C^t_{ur}) = \phi(M_{\rm HI})|_{C_{ur}>C^t_{ur}}. \quad (3)$$

This represents the HIMF for galaxies which have a colour C_{ur} redder than a threshold value C^t_{ur}. Similarly, we define the luminosity-conditioned HIMF as

$$\phi(M_{\rm HI}|M^t_r) = \phi(M_{\rm HI})|_{M_r<M^t_r}, \quad (4)$$

which represents the HIMF for galaxies which are more luminous than a threshold value M^t_r. To compute the conditional HIMF, we start with the full sample of 7709 galaxies and create a subsample based on a threshold colour C^t_{ur} (or magnitude threshold M^t_r). We compute the HIMF for this subsample and also estimate its errors as outlined in Section 3. We then fit a Schechter function to obtain a conditional HIMF for the particular subsample. We repeat this exercise to obtain the conditional HIMF as a function of ${C_{ur}}^t$ and M^t_r. Our results are shown in Figs 1 and 2.

For the rest of the paper, the values of the characteristic mass M_* and the amplitude of the Schechter function ϕ_* (in equation 2) will be in the units $[\log(M_*/M_\odot) + 2\log h_{70}]$ and $\left[10^{-3}h^3_{70}Mpc^{-3}{\rm dex}^{-1}\right]$, respectively. We will also quote $M_{\rm H\,I}$ in the same units as M_*.

In the left-hand panel of Figs 1 and 2, we show the Schechter function fits to the conditional HIMF. The thick solid line is the HIMF

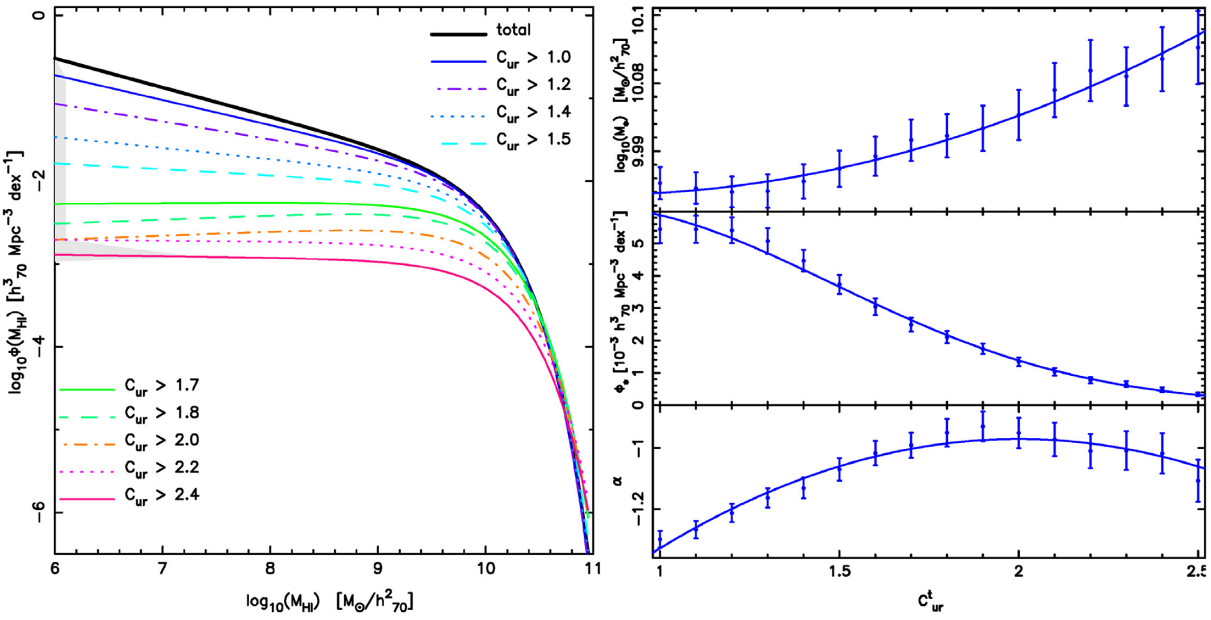

Figure 1. *Left*: Conditional HIMF as a function of increasing colour thresholds (top to bottom). The thick solid line is the HIMF for the full sample. The shaded grey region does not contain data, the conditional HIMF have, however, been extrapolated into this regime as well. *Right*: The Schechter function parameters of the conditional HIMF and their uncertainties as a function of colour thresholds. The solid lines are fits to the data points with a quadratic function. The top, middle, and bottom panels show the dependence of M_*, ϕ_* and α, respectively, on the colour threshold $C^{\rm t}_{ur}$.

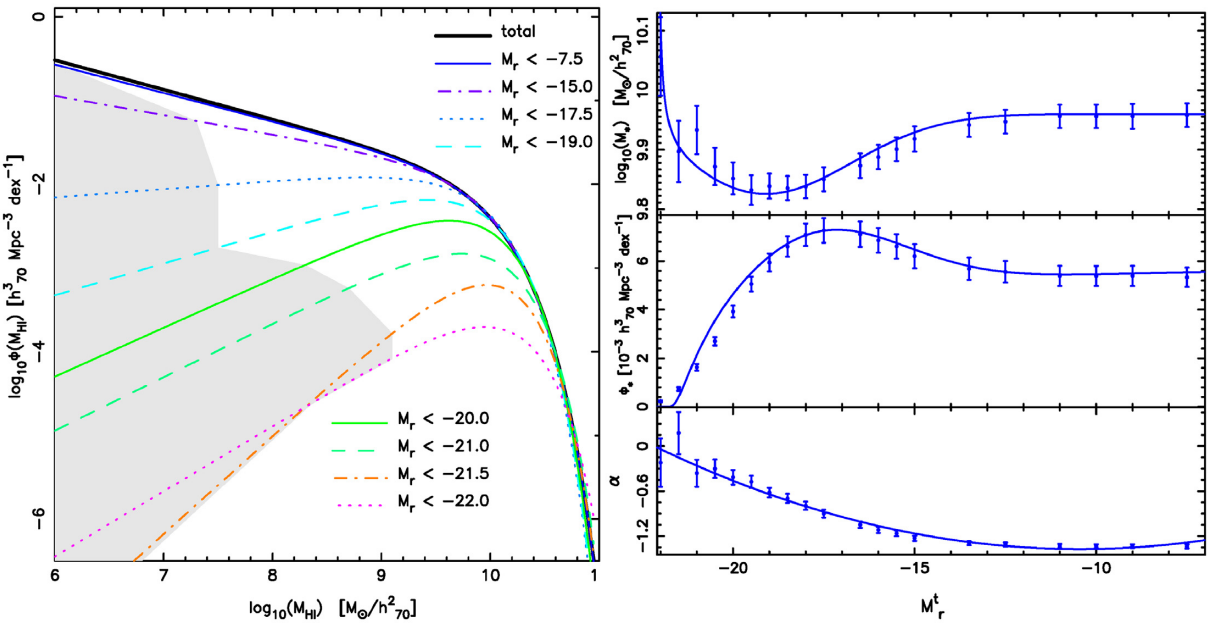

Figure 2. *Left*: Conditional HIMF as a function of decreasing rest frame magnitude thresholds (top to bottom). The thick solid line is the HIMF for the full sample. The shaded grey region does not contain data; the conditional HIMF have, however, been extrapolated into this regime as well. *Right*: The Schechter function parameters of the conditional HIMF and their uncertainties as a function of magnitude thresholds M^t_r. The solid lines are fits to the data points. For α (bottom), we fit with a quadratic function. For M_* (top) and ϕ_* (middle), we fit with a function of the form: $y(x) = \left[a + b\exp\left(-\frac{(x+c)^2}{2d}\right)\right]\frac{f}{(x+e)}$.

for the full sample. The shaded grey patch represents the region where there is no data. While displaying the Schechter functions we have, however, extrapolated them to this region as well. The right-hand panels represent the Schechter function fits and their uncertainties. The lines represent a parametric fit to these values. We note that the errorbars on the Schechter function parameters, although representative of the sample, are correlated, since the sample at each threshold (i.e. C^t_{ur} or M^t_r) contains the sample of the previous neighbouring threshold.

In Fig. 1, we look at the colour-conditioned HIMF and its dependence on the threshold colour C^t_{ur}. For $2.0 \leq C^t_{ur} \leq 2.4$, the slope at the low-mass end is flat, or $\alpha \sim -1$ (see bottom right panel of Fig. 1). At this end the amplitude, ϕ_* is small (16 × smaller) compared to the amplitude of the total HIMF, $\phi_* = 5.3 \times 10^{-3}$, but

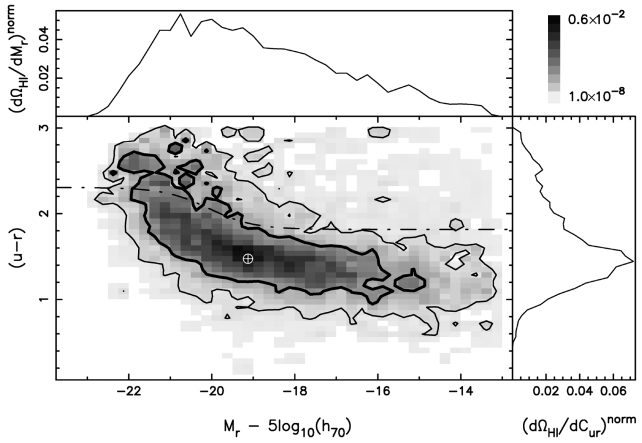

Figure 3. The bottom left panel shows the distribution function $p(\Omega_{\rm H\,I})$ (see equation 7) in the CM plane colour-coded by $(\Omega_{\rm HI}^{ij})^{\rm norm}$ (equation 9). The thick (thin) line represents the 1σ (2σ) widths of $p(\Omega_{\rm H\,I})$. The dash–dotted line separates the optical red (above) and blue (below) populations (Baldry et al. 2004). The top left (bottom right) panel is the marginalized distribution of $\Omega_{\rm H\,I}$ as a function of M_r (C_{ur}). The crossed circle represents the peak of the two-dimensional distribution function, $p(\Omega_{\rm H\,I})$.

the characteristic mass $M_* = 10.13$ is about 50 per cent larger than that of the HIMF of the full sample. A large value of C_{ur}^t means that the subsample contains mostly redder galaxies. By decreasing this value, we add blue galaxies to the sample and the conditional HIMF then approaches the total HIMF in the limit $C_{ur}^t \Rightarrow -\infty$. In our sample, this is achieved when $C_{ur}^t = 0$. As can be seen in Fig. 1, there is a near monotonic change in the shape (with the exception of α) of the conditional HIMF with C_{ur}^t. Although α as a function of C_{ur}^t peaks at about $C_{ur}^t = 1.9$, the variation is still consistent with a constant value beyond that. Incidentally the peak in α occurs close to the value of the optimal divider of Baldry et al. (2004) at $C_{ur} = 2.3$ (see Fig. 3). The red population dominates the HIMF at the large mass end whereas decreasing the C_{ur}^t we progressively add bluer galaxies to our sample which start to dominate the knee and then the low-mass end for even smaller values of C_{ur}^t.

In Fig. 2, we look at the dependence of the conditional HIMF on M_r^t. Unlike the previous case, the dependence of the conditional HIMF on M_r^t is not monotonic (see right-hand panel of Fig. 2). We see a dip (bump) in M_* (ϕ_*) at $M_r^t = 19$ ($M_r^t \sim 17.5$). Coincidentally, the distribution of the blue (red) population of galaxies is centred at $M_r = 19$ ($M_r = 20$) (see fig. 3 of D20). As we move from the luminous ($M_r^t \leq 20$ dominated by the red sample), to the faint end, the conditional HIMF picks the contribution from the blue cloud at $M_r = 19$. The bimodality of the underlying optical galaxy sample is reflected more strongly in the luminosity-conditioned HIMF than the colour-conditioned HIMF.

4.2 The distribution of $\Omega_{\rm H\,I}$ in the C_{ur}–M_r plane

We extend our previous definition to the two-dimensional conditional HIMF:

$$\phi(M_{\rm HI}|C_{ur}^t, M_r^t) = \phi(M_{\rm HI})|_{(C_{ur}>C_{ur}^t),(M_r<M_r^t)}. \quad (5)$$

This represents the HIMF of galaxies redder than C_{ur}^t and more luminous than M_r^t, for which the corresponding H I density parameter is

$$\Omega_{\rm HI}(C_{ur}^t, M_r^t) = \frac{1}{\rho_c}\int_0^\infty M_{\rm HI}\phi(M_{\rm HI}|C_{ur}^t, M_r^t)dM_{\rm HI}. \quad (6)$$

In our sample $\Omega_{\rm HI}(C_{ur}^t, M_r^t) = \Omega_{\rm HI}^{\rm tot} = 4.894 \times 10^{-4}$ when $C_{ur}^t = 0.0, M_r^t = -6.0$. We compute 2500 conditional HIMFs and their associated errors in the CM plane by dividing $C_{ur}^t \in [3.0, 0.0]$ (decreasing colour threshold) and $M_r^t \in [-23.0, -6.0]$ (increasing magnitude threshold) into 50 bins each. From equation (6), we see that the variation of $\Omega_{\rm HI}(C_{ur}^t, M_r^t)$ is that of a cumulant in the two-dimensional CM plane. If we define the normalized conditional H I density parameter as $\Omega_{\rm HI}^{\rm norm}(C_{ur}^t, M_r^t) = \frac{\Omega_{\rm HI}(C_{ur}{}^t, M_r^t)}{\Omega_{\rm HI}^{\rm tot}}$, then $\Omega_{\rm HI}^{\rm norm}(C_{ur}^t, M_r^t)$ is bounded and varies from 0 (luminous red, top left corner of Fig. 3) to 1 (faint blue, bottom right corner of Fig. 3).

We define the distribution function of the cosmological H I density parameter in the CM plane

$$p\left(\Omega_{\rm HI}(C_{ur}, M_r)\right) = \left.\frac{\partial^2\Omega_{\rm HI}^{\rm norm}(C_{ur}{}^t, M_r^t)}{\partial C_{ur}^t \partial M_r^t}\right|_{[C_{ur}^t=C_{ur}, M_r^t=M_r]}. \quad (7)$$

By construction this is a normalized distribution

$$\int\int p\left(\Omega_{\rm HI}(C_{ur}, M_r)\right) {\rm d}C_{ur}{\rm d}M_r = 1.0. \quad (8)$$

The cosmological H I density in a given CM (ji) pixel is

$$(\Omega_{\rm HI}^{ij})^{\rm norm} = \int_{M_r{}^i}^{M_r{}^{i+1}}\int_{C_{ur}{}^j}^{C_{ur}{}^{j+1}} p\left(\Omega_{\rm HI}(C_{ur}, M_r)\right) {\rm d}C_{ur}{\rm d}M_r. \quad (9)$$

In Fig. 3, we plot the distribution function, $p(\Omega_{\rm H\,I})$, of the cosmological H I density parameter in the CM plane. Each pixel is colour-coded to the $(\Omega_{\rm HI}^{ij})^{\rm norm}$ value. The top left (bottom right) panel shows the marginalized distribution of $\Omega_{\rm H\,I}$ as a function of magnitude (colour). The dot–dashed line is the optimal divider which classifies these galaxies into red and blue populations (Baldry et al. 2004). The thick (thin) contour is the 1σ (2σ) width of the distribution function, $p(\Omega_{\rm H\,I})$ [i.e. the contour is determined from equation 8 by setting the RHS to 0.68 (0.95)]. The crossed circle is the peak of $p(\Omega_{\rm H\,I})$ in two dimensions, and does not match the peak of the marginalized distribution because it is skewed.

5 DISCUSSION

In this paper, we have presented the conditional HIMF, conditioned on colour and/or magnitude. Based on the conditional HIMF, we obtained the distribution of $\Omega_{\rm H\,I}$, $p(\Omega_{\rm H\,I})$, in the CM plane of galaxies. Not surprisingly our results for $\phi(M_{\rm HI})|_{M_r<-21}$ and even brighter thresholds is similar to those obtained for the conditional HIMF, $\phi(M_{\rm HI})|_{M_{\rm star}\geq 10}$, for massive galaxies (Lemonias et al. 2013) from the GASS survey (Catinella et al. 2010, 2012); this is because the stellar mass of galaxies is correlated with its luminosity.

Both the two-dimensional and marginalized distributions show that they have long tail towards faint blue galaxies and luminous red galaxies. The peak of $p(\Omega_{\rm H\,I})$ in the CM plane occurs at $C_{ur}{}^{\rm max} = 1.44, M_r{}^{\rm max} = -19.25$ in the blue cloud, which is about 1.36 mag fainter than the characteristic luminosity of blue galaxies in SDSS (Baldry et al. 2004). The width of $p(\Omega_{\rm H\,I})$ is also fairly broad in both colour and magnitude; the average 1σ (2σ) widths being $\sigma_{\rm C} = 0.8$ and $\sigma_{\rm M} = 3.0$ ($\sigma_{\rm C} = 1.1$, $\sigma_{\rm M} = 4.8$). At the fainter end, $M_r > -16$, ~ 10 per cent of $\Omega_{\rm HI}^{\rm tot}$ is locked in gas-rich low surface brightness galaxies. The red population, on the other hand, contributes ~ 18 per cent to the H I budget.

The CM plane can be thought of as a coordinate system in which we can plot distributions of other cosmological density parameters (related to galaxies), $p(\Omega_{\rm X})$ where X denotes a property, e.g. stellar mass $M_{\rm star}$, SFR, molecular hydrogen mass $M_{\rm H_2}$, which in turn are computed from $\phi(X|C_{ur}{}^t, M_r^t)$. We therefore have all the

information needed to obtain the mean relation between different galaxy properties by discarding the common coordinate system. We emphasize that this relation is unbiased and represents the underlying relation since the distributions have folded in the survey selection. The blind nature of the survey is also important since there is no selection bias in estimating $\phi(X)$. This can be repeated for different galaxies populations (blue or red) and for other bands as well. The methods outlined in this paper are statistical in nature and provide a powerful and unbiased way to probe the multivariate distributions of galaxy populations. We will report on the mean H I–stellar mass relation in a forthcoming paper.

ACKNOWLEDGEMENTS

We would like to thank R. Srianand, A. Paranjape, and J. S. Bagla for useful discussions. NK acknowledges the support of the Ramanujan Fellowship[1] and the IUCAA[2] associateship programme. All the analyses were done on the XANADU and CHANDRA servers funded by the Ramanujan Fellowship.

We thank the entire ALFALFA collaboration in observing, flagging, and extracting the properties of galaxies that this paper makes use of. This work also uses data from SDSS DR7. Funding for the SDSS and SDSS-II has been provided by the Alfred P. Sloan Foundation, the Participating Institutions, the National Science Foundation, the U.S. Department of Energy, the National Aeronautics and Space Administration, the Japanese Monbukagakusho, the Max Planck Society, and the Higher Education Funding Council for England. The SDSS Website is http://www.sdss.org/. The SDSS is managed by the Astrophysical Research Consortium for the Participating Institutions.

DATA AVAILABILITY

The data used in this work is publicly available. SDSS DR7 (Abazajian et al. 2009) data can be accessed from *sciserver.org* and the $\alpha.40$ (Haynes et al. 2011) data from ALFALFA can be accessed from *egg.astro.cornell.edu*.

REFERENCES

Abazajian K. N. et al., 2009, ApJS, 182, 543
Baldry I. K. et al., 2004, ApJ, 600, 681
Blanton M. R., Roweis S., 2007, AJ, 133, 734
Catinella B. et al., 2010, MNRAS, 403, 683
Catinella B. et al., 2012, A&A, 544, A65
Dutta S., Khandai N., Dey B., 2020, MNRAS, 494, 2664 (D20)
Haynes M. P. et al., 2011, AJ, 142, 170
Haynes M. P. et al., 2018, ApJ, 861, 49
Jones M. G., Haynes M. P., Giovanelli R., Moorman C., 2018, MNRAS, 477, 2
Kennicutt R. C., 1989, ApJ, 344, 685
Kennicutt R. C., 1998, ApJ, 498, 541
Lemonias J. J., Schiminovich D., Catinella B., Heckman T. M., Moran S. M., 2013, ApJ, 776, 74
Loveday J., 2000, MNRAS, 312, 557
Martin A. et al., 2010, ApJ, 723, 1359
Morganti R. et al., 2006, MNRAS, 371, 157
Oosterloo T. A., Morganti R., Sadler E. M., van der Hulst T., Serra P., 2007, A&A, 465, 787
Schmidt M., 1959, ApJ, 129, 243

[1]Awarded by the Department of Science and Technology, Government of India.
[2]Inter University Centre for Astronomy and Astrophysics, Pune, India.

Schmidt M., 1963, ApJ, 137, 758
Serra P., et al., 2012, MNRAS, 422, 1835
Zwaan M. A., Briggs F. H., Sprayberry D., 2001, MNRAS, 327, 1249
Zwaan M. A. et al., 2003, AJ, 125, 2842

This paper has been typeset from a TEX/LATEX file prepared by the author.